Journal of Catalysis 287 (2012) iii–viii

Contents lists available at SciVerse ScienceDirect

Journal of Catalysis

journal homepage: www.elsevier.com/locate/jcat

Journal of Catalysis Vol. 287, 2012

Contents

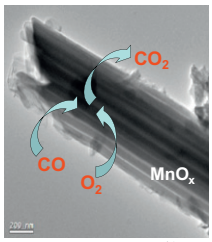

Non-stoichiometric Mn-oxide (MnO_x) with high specific surface area (525 m^2 g^{-1}) shows high catalytic activity in CO oxidation reaction.

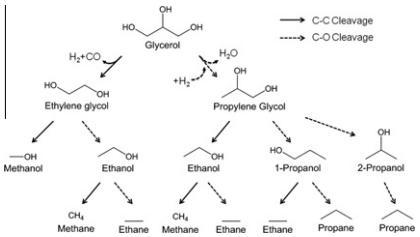

The major reaction pathways for aqueous-phase reforming of glycerol show the dependence of product selectivity on C–C bond cleavage (metal site-based) vs. C–O bond cleavage (acid site-based).

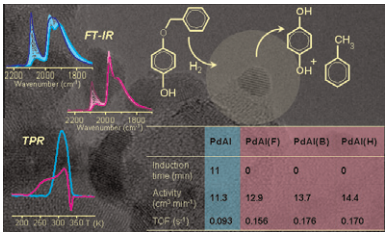

Relationships between the reduction state of a supported palladium catalyst, its surface structural properties, and its catalytic performance are investigated in a multi-technique approach.

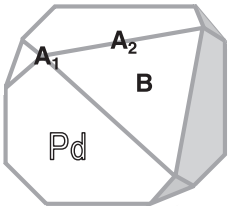

A_1: Active for H_2O formation,
inactivated by H^+ and Br^- adsorption.
A_2: Active for H_2O_2 formation,
Langmuir-Hinshelwood mechanism.
Major sites on Pd-PVP catalyst.
B : Active for H_2O_2 formation,
first order on H_2 partial pressure.

Kinetics of the direct H_2O_2 synthesis from H_2 and O_2 and Br^- adsorption behaviors on a Pd–PVP colloid catalyst in water containing H^+ and Br^- ions was quite different from those on a Pd/C catalyst, which proposed improved classification of Pd surface sites active for the H_2O_2 synthesis.

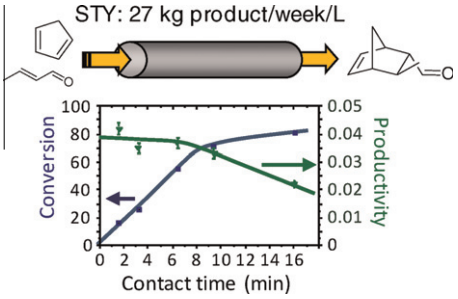

Aluminum oxide–grafted silica monoliths were proved as highly productive catalytic microreactors for the in-flow implementation of the Diels–Alder reaction. Control of contact time and monolithic length has allowed to overcome external diffusion limitations.

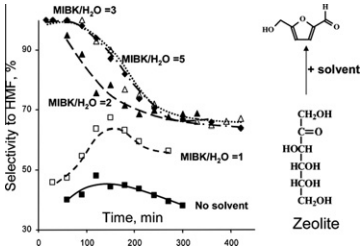

Solvent addition significantly improved the selectivity to HMF in the aqueous phase dehydration of fructose over zeolite catalysts. The solvent not only improves the selectivity by extraction of the HMF produced, but also changes the intrinsic activity of the catalyst.

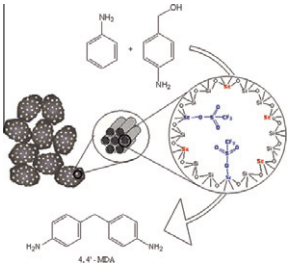

Isolated scandium triflate species incorporated in a UVM-7 porous bimodal support were prepared using a two-step strategy. These catalysts showed a high selectivity in the synthesis of 4, 40-methylenedianiline from aniline and 4-aminobenzylalcohol under mild conditions.

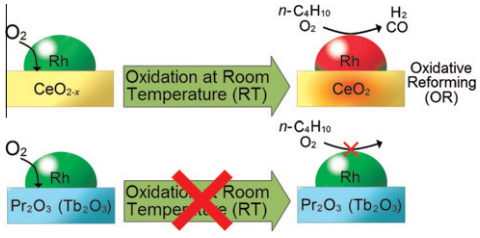

Oxidative reforming of *n*-butane was triggered rapidly at room temperature over Rh/CeO_{2-x} but not over Rh/Pr_2O_3 and Rh/Tb_2O_3. The unique ability of CeO_{2-x}, unlike Pr_2O_3 and Tb_2O_3, to be oxidized at room temperature played a crucial role in triggering oxidative reforming at room temperature.

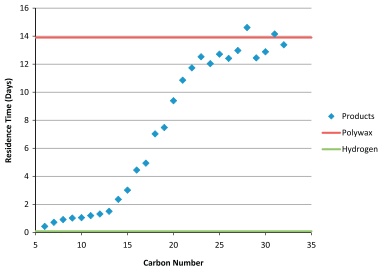

Residence time increase with carbon number up to C_{22}, the major removal method for products lighter than C_{10} is the gas phase while products between C_{10} and C_{22} are removed by both the vapor and the liquid flow. Products heavier than C_{22} have the same residence time as the polywax.

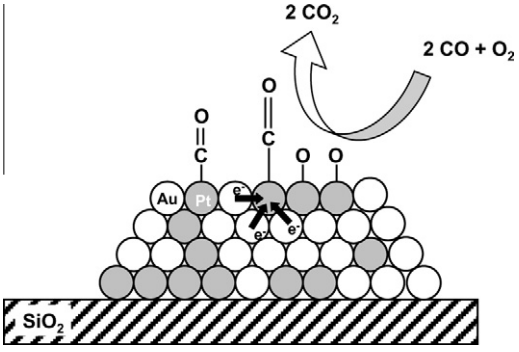

A promoting effect of Au is reported on the kinetics of CO oxidation over Pt on AuPt bimetallic nanoparticles supported on SiO_2. This is attributed to a greater electron density of the Pt surface atoms due to charge transfer from Au to Pt, as indicated by XPS and CO-FTIR.

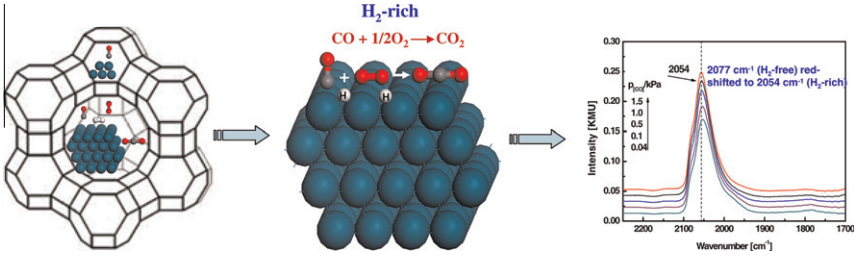

Mechanistic study of PROX of CO was carried out over a Pt(1.0 wt.%)/NaY zeolite catalyst from 300 to 523 K by combination of kinetics and spectroscopy. The activity of CO oxidation at 300 K was assumed to originate from Pt clusters less than 1.0 nm. In the presence of H_2, a significant red-shift of the CO stretch frequency was observed in DRIFT spectra and CO oxidation was significantly enhanced.

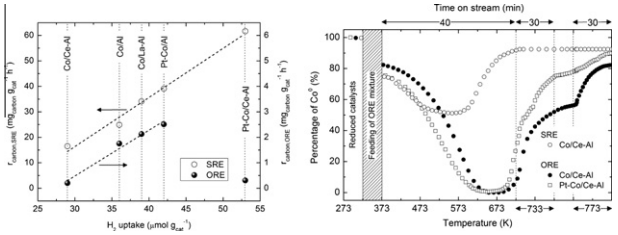

Temperature- and spatial resolved XANES indicated that the nature of supports and the composition of reactants determine the Co^{2+}/Co^0 ratio in reforming of ethanol, which control the activity and deposition of carbon.

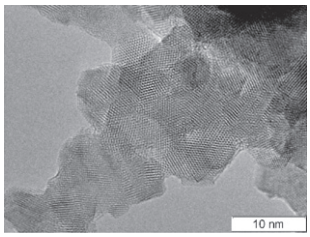

$$2C_2H_5OH + O_2 \xrightarrow[CdS]{2h\nu} 2CH_3CHO + 2H_2O$$

$$2(CH_3)_2CHOH + O_2 \xrightarrow[CdS]{2h\nu} 2(CH_3)_2CO + 2H_2O$$

Nanosized cadmium sulfide photocatalyzes partial oxidation of alcohol vapors with oxygen of air at room temperature under visible light with quantum efficiency up to 6.6%.

Nanosized cadmium sulfide photocatalyzes partial oxidation of alcohol vapors with oxygen of air at room temperature under visible light with quantum efficiency up to 6.6%.

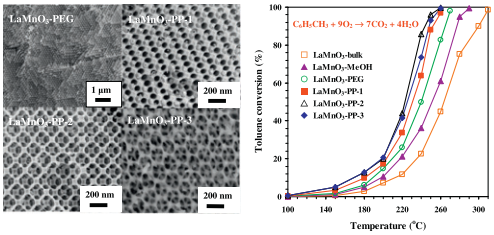

Through the surfactant-assisted PMMA-templating method, we prepared three-dimensionally ordered macroporous (3DOM) $LaMnO_3$ catalysts with nanovoid skeletons. It is found that the excellent performance of the catalysts in toluene combustion can be related to the high surface area and oxygen adspecies concentration as well as low-temperature reducibility of 3DOM $LaMnO_3$.

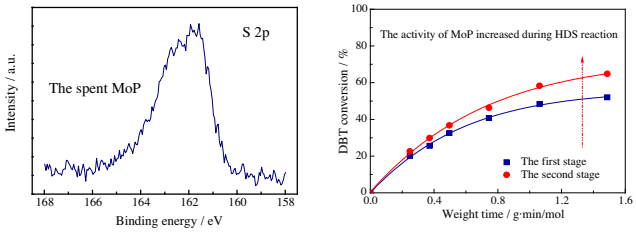

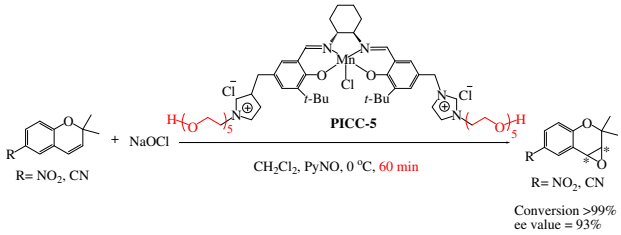

PEG chain-modified ionic liquid functionalized chiral salen Mn(III) complexes with built-in phase-transfer capability were first prepared and proved highly efficient in the asymmetric epoxidation of unfunctionalized olefins using aqueous NaOCl as an oxidant.

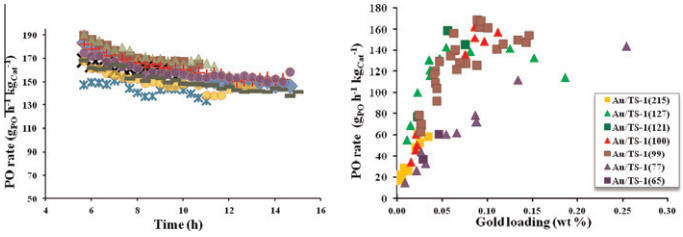

The Au/TS-1 catalysts prepared at optimal DP conditions (pH of the gold slurry solution, the mixing time, and the preparation temperature) showed a PO rate ~ 160 $g_{PO}h^{-1}kg_{Cat}^{-1}$, which is the highest PO rate at 200 °C yet reported. Instead of using TS-1 with high Ti content to increase the site density, diluted systems (low Au loading/low Ti loading) are recommended for preparing highly active Au/TS-1 for PO production.

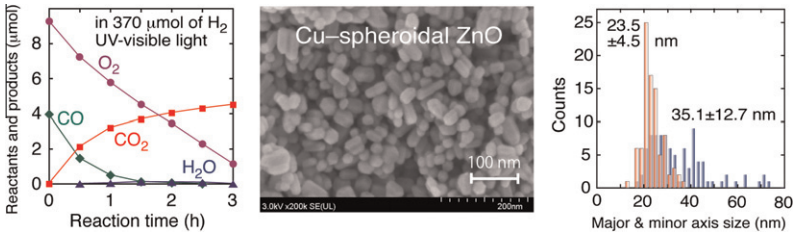

Photo-PROX: Preferential oxidation of CO in H_2 by photocatalysis using Cu(II) on spheroidal ZnO as the catalyst.

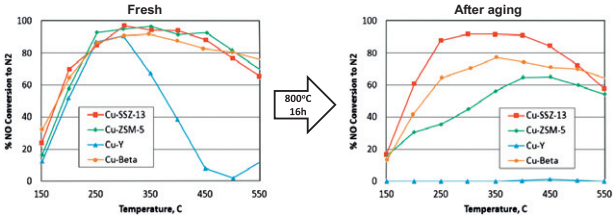

After hydrothermal aging at 800 °C for 16 h, the NO_x reduction performance of Cu-ZSM-5, Cu-beta and Cu-Y were significantly reduced, while that of Cu-SSZ-13 was not affected.

LETTER TO THE EDITOR

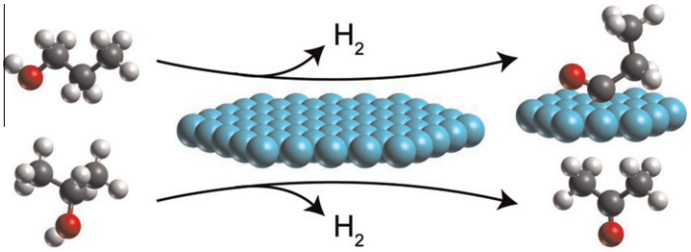

The experimentally observed dissimilar dehydrogenation behavior of 1- and 2- propanol on Pt surfaces is rationalized via DFT model calculations. The most stable dehydrogenation product of the primary alcohol, propionyl, strongly adsorbs whereas for the secondary alcohol, acetone is determined as product which desorbs easily.